ACS APPLIED MATERIALS & INTERFACES

Research Article

www.acsami.org

Measuring the Elastic Modulus of Thin Polymer Sheets by Elastocapillary Bending

Jinhye Bae, Tetsu Ouchi, and Ryan C. Hayward*

Polymer Science and Engineering Department, University of Massachusetts Amherst, Amherst, Massachusetts 01003, United States

Supporting Information

ABSTRACT: We describe bending by liquid/liquid or liquid/air interfaces as a simple and broadly applicable technique for measuring the elastic modulus of thin elastic sheets. The balance between bending and surface energies allows for the characterization of a wide range of materials with moduli ranging from kilopascals to gigapascals in both vapor and liquid environments, as demonstrated here by measurements of both soft hydrogel layers and stiff glassy polymer films. Compared to existing approaches, this method is especially useful for characterizing soft materials (<megapascals in modulus), thin sheets with sub-millimeter in-plane dimensions, and samples immersed in a variety of liquid media. The measurement is independent of the three-phase (liquid/solid/medium) contact angle for appropriately chosen wetting conditions, therefore requiring only knowledge of the liquid/medium surface tension and the sheet thickness to characterize sheets with specified shapes. Using the method, we characterize photo-cross-linkable polyelectrolyte hydrogel sheets swelled to equilibrium in an aqueous medium and demonstrate good agreement with predicted scalings of the modulus and swelling ratio with cross-link density.

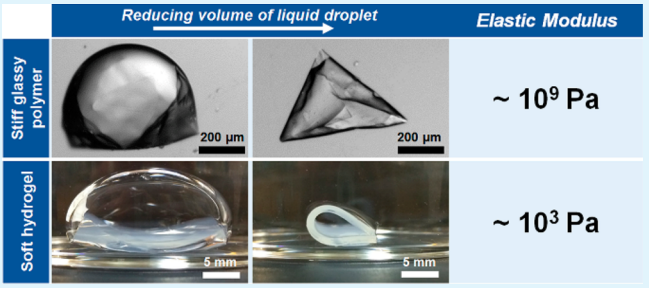

KEYWORDS: *surface tension, modulus, bending, hydrogels, thin film*

INTRODUCTION

Flexible elastic sheets present a rich array of basic questions in mechanics,[1−4] and offer applications in areas such as biomaterials and stimuli-responsive devices.[5−8] However, while knowledge of the elastic properties of these materials is critical for understanding and controlling their behavior, classical macroscopic methods such as tensile or compression testing, or shear rheology are often poorly suited for characterizing thin and highly compliant membranes. When the materials are limited to small in-plane sizes, or need to be studied while immersed in a liquid medium, traditional testing methods are further complicated.

A number of methods have been developed in recent years to address these limitations on the mechanical characterization of compliant materials on small scales. Nanoindentation, frequently conducted with an atomic force microscope (AFM) tip, has become a valuable tool for measuring the local elastic properties of nano- to microscale soft objects such as thin polymer films,[9−11] gels,[12−14] and cells.[15−20] However, interpretation of data from this technique often leads to model-dependent conclusions that are complicated by the presence of adhesion between the tip and the sample, by viscoelastic and/or poroelastic relaxation processes, and by effects from underlying rigid substrates.[9,20,21] Microtensile[22−24] and bulge tests[25,26] have been successfully exploited for mechanical characterization of thin films with small in-plane dimensions but often require significant efforts in micromachining to prepare appropriately mounted samples, or otherwise require handling and fixing of small and flexible specimens. Aspiration methods based on measuring the deformation of a sample pulled into a capillary by a known hydrostatic pressure are also useful but have so far been applied only to nearly spherical samples.[27−31] Cavitation rheology—a measurement of the pressure needed to form a bubble of fluid in a material—is especially promising due to its simplicity and flexibility, though so far has not been applied to thin layers and can be complicated for brittle materials where fracture precedes elastic cavitation.[32−34] Wrinkling of thin films supported on soft and thick elastic substrates,[35] or floating on liquid surfaces[36] has been exploited to quantitatively characterize elastic properties of thin films, and very recently, tensile testing of thin films floating on the surface of water was reported.[37] However, these techniques generally require films with in-plane dimensions of several millimeters and elastic moduli in the range of megapascals to gigapascals.

Here, we report a simple approach for characterizing the elastic modulus of soft materials and thin films that takes advantage of bending driven by interfacial tension, inspired by previous work on capillary folding of polymer sheets.[38] The balance between interfacial tension γ and bending stiffness B of an elastic sheet is described by the elastocapillary bending length $L_{EC} = (B/\gamma)^{1/2}$, where $B = \bar{E}h^3/12$ for a homogeneous isotropic film with plane-strain modulus $\bar{E}$ and thickness h.

Received: March 24, 2015
Accepted: June 22, 2015
Published: July 2, 2015

DOI: 10.1021/acsami.5b02567
ACS Appl. Mater. Interfaces 2015, 7, 14734−14742

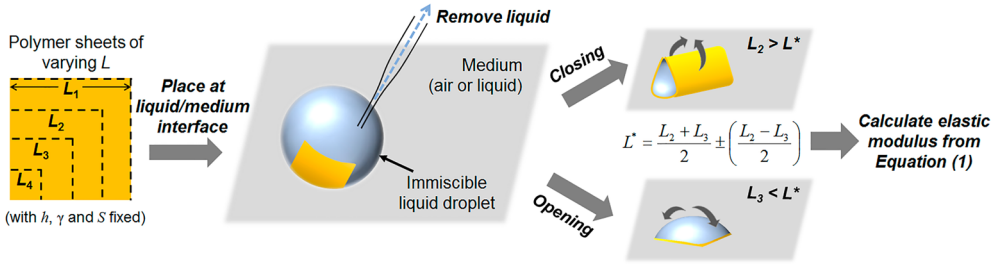

Figure 1. Schematic illustration of elastocapillary bending method for measurement of the elastic modulus of a thin polymer sheet.

When the in-plane size of the sheet is comparable to L_{EC}, interfacial tension between a liquid droplet and the surrounding medium is just sufficient to bend the material, providing a very simple means to determine $\bar{E}$ of the solid film. For appropriate wetting conditions, this condition does not depend on the contact angle of the solid/liquid/medium interface, meaning that the method requires separate measurements of only the liquid/medium interfacial tension, and the sheet thickness. We demonstrate here that the technique is suitable for measuring materials over a broad range of moduli (from kilopascals to gigapascals), including those with small in-plane dimensions, and immersed in liquid media as well as air.

EXPERIMENTAL SECTION

Materials and Polymer Synthesis. Poly(*p*-methylstyrene) (PpMS) containing pendent benzophenone photo-cross-linkers and poly(*N*-isopropylacrylamide-*co*-acrylamidobenzophenone-*co*-acrylic acid-*co*-rhodamine B-methacrylate) (PNIPAM copolymer) were synthesized by free-radical polymerization at 80 °C in 1,4-dioxane for 15 h following 3 freeze−pump−thaw cycles and a nitrogen purge using recrystallized azobis(isobutyronitrile) (AIBN, Aldrich) as initiator, as described in more detail previously.[39] Polymers were purified by precipitation into stirring diethyl ether (for PNIPAM) or methanol (for PpMS), washed by filtration, and dried in a vacuum oven overnight. Concentrations of monomers and initiator in solvent were chosen as follows: 3 g of *N*-isopropylacrylamide (NIPAm; Tokyo Chemical Industry Co., Ltd.), 533 mg of acrylamidobenzophenone (AAmBP), 114.5 L of acrylic acid (AAc), 47.6 mg of rhodamine B-methacrylate (RhBMA), and 5 mg of AIBN in 30 mL of 1,4-dioxane, resulting in a copolymer with 7 mol % AAmBP, 5.5 mol % AAc, and 0.3 mol % RhBMA; 3 mL of *p*-methylstyrene (pMS; Aldrich), 0.45 g of AAmBP, and 0.015 g of AIBN in 30 mL of 1,4-dioxane, resulting in a copolymer containing 10 mol % AAmBP. Polymer compositions were confirmed by ^{1}H NMR spectroscopy (Bruker DPX300).

Polyacrylamide (PAAm) hydrogels were synthesized using 1000 μL of an aqueous pregel solution containing 660 mM acrylamide (Aldrich), 19.8 mM bis(acrylamide) (Research Organics), and 25 μL of 3.4 wt % 2,2′-azobis[2-methyl-*N*-(2-hydroxyethyl)propionamide] aqueous solution as the photoinitiator (VA-086, Wako Pure Chemical Industries, Ltd.). The degassed pregel solution was inserted between two (tridecafluoro-1,1,2,2-tetrahydrooctyl)dimethylchlorosilane (Gelest) treated glass slides separated by 1 mm spacers. Gelation was induced by exposure to UV light (wavelength, 365 nm) for 20 min, followed by immersion in deionized water for 2−3 days to fully swell the gel and remove unreacted monomers.

Preparation of Photo-cross-linkable Polymer Sheets. To prepare copolymer films, 3 wt % poly(sodium acrylate) (Sigma-Aldrich; M_w = 30 kg/mol) was spin-coated onto a precleaned 1 × 1 cm^2 silicon substrate, yielding a film of ∼100 nm thickness. The residual solvent was evaporated on a 150 °C hot plate for 2 h, and then the film was soaked in 1.35 M $CaCl_2$ solution for 20 s to form a Ca^{2+}-cross-linked sacrificial layer.[40]

Films of PpMS with thicknesses of 120 and 670 nm were prepared by spin-casting (2 krpm) of 20 and 100 mg/mL PpMS solutions in toluene onto the sacrificial layer, respectively. Films of PpMS with thicknesses of 2 μm were prepared via drop-casting of 30 μL of PpMS solution in toluene (10 mg/mL) on the sacrificial layer, and the solvent was slowly removed for 5 h at 68 °C in a closed glass bottle (0.13 oz capacity glass jar, Freund Container). To prepare PNIPAM copolymer sheets, a 100 μL drop of copolymer solution in chloroform (1 wt %) was drop-cast on the sacrificial layer, and the solvent was slowly evaporated for 5 h at 50 °C in a closed glass bottle (0.13 oz capacity glass jar, Freund Container). The film thickness was measured using a stylus profilometer (Dektak, Veeco).

Square and triangular mask patterns with a variety of side lengths were designed in AutoCAD (AutoDesk) and printed on transparent photomasks (Front Range PhotoMask). The PpMS and PNIPAM copolymer films were cross-linked by using an epi-fluorescence microscope (Zeiss Axiovert 200) and a homemade mask aligner. Films were exposed to 120 J cm^{-2} of UV light (X-Cite Series 120, Lumen Dynamics; excitation filter, 365 nm) through the photomask to fully cross-link PpMS and 3−30 J cm^{-2} to partially cross-link PNIPAM, using a 10× objective. UV doses are measured using an X-Cite XR2100 power meter (Lumen Dynamics) at 365 nm.

The PpMS and PNIPAM sheets were submerged in a solvent mixture of toluene:hexane = 1:0.6, and water:ethanol = 1:2, respectively, to dissolve un-cross-linked portions and then immersed in an aqueous medium (containing 1 mM NaCl, and 1 mM phosphate buffer, pH 7.2) to dissolve the sacrificial layer, release the films, and induce swelling in the case of the PNIPAM films.

Elastocapillary Bending Test. For each material system, a series of samples with square or equilateral triangular shapes of varying side lengths L was first prepared. For samples measured in liquid media, a given polymer film was immersed into the desired medium, and a droplet of the immiscible probe liquid with a size much larger than the lateral dimensions of the film was introduced into the liquid medium using a glass pipet. Subsequently, the sample was placed at the interface between the droplet and medium, making sure that all edges of the film were adsorbed to the interface, using either tweezers or a tapered glass capillary to position the sample. For samples measured in air, a large droplet of the probe liquid was pipetted directly onto the polymer film surface, with care to ensure that the three-phase contact line wetted each edge of the film. Next, the volume of liquid droplet was reduced by pipetting, causing the polymer film at the interface to bend. Droplet suction for millimeter-sized films was conducted using a 5 $^3/_4$ in. glass pasteur pipet with a latex bulb, while for smaller samples, a cylindrical glass capillary (1 mm outer and 0.6 mm inner diameters, World Precision Instruments) was tapered to a sharp tip (∼10 μm diameter) using a Narishige PC-10 micropipette puller and MF-900 microforge, then connected to a syringe pump. For each sample, it was noted whether the film was bent into a "closed" state with opposite edges or corners in contact (corresponding to $L > L^*$), or whether the film reopened without ever reaching the closed state ($L < L^*$).

In most cases, h, γ, and the shape (S) were held fixed, while films with varying L were measured as shown in Figure 1, with the value of L^* estimated as the average between the smallest L that yielded a closed state and the largest L that did not (with an uncertainty of plus-or-minus half of the difference between these two values of L). Finally, $\bar{E}$ of the material was estimated from

$$\bar{E} = \frac{12\gamma}{h^3}\left(\frac{L^*}{S}\right)^2 \quad (1)$$

DOI: 10.1021/acsami.5b02567
ACS Appl. Mater. Interfaces 2015, 7, 14734−14742

More generally, if two or more of the variables L, h, S, and γ are varied, we use eq 1 with L in place of L^* to estimate either an upper bound on $\overline{E}$ for samples that did reach a closed state or a lower bound for samples that did not. In this case, $\overline{E}$ is estimated as the average of these two bounds (with an uncertainty of plus-or-minus half of the difference between the two). For all materials tested here, only L was varied in a given measurement of $\overline{E}$, except in the case of photo-cross-linkable PNIPAM sheets, where samples with variable L, h, and S were used.

Characterization. Micrographs and movies of elastocapillary bending of Kapton films were taken using a digital camera (PowerShot A640, Canon). For PpMS and PNIPAM films, fluorescence and bright field optical micrographs and movies were obtained using a Zeiss Axiovert 200 inverted optical microscope with a 2.5× objective, and a QImaging camera (Retiga-2000R).

Nanoindentation tests were performed in ambient conditions by using a TriboIndenter (Hysitron Inc.) with a Berkovich diamond tip. A trapezoidal loading profile with different loading rates of 10, 25, and 100 μN/s and a constant peak load of 500 μN with a hold period of 5 s were applied to photo-cross-linked PpMS films ($h \sim 100$ μm). Reduced moduli were calculated based on the portion of the unloading curves between 95% and 20% of the maximum force using the Oliver and Pharr analytical model.[41]

PNIPAM samples for UV/vis absorption spectroscopy were drop-cast by placing 200 μL of copolymer solution in chloroform (1 wt %) onto UV-ozone treated 1 × $^1/_2$ in.^{2} quartz plates, and the solvent was slowly evaporated for 5 h at 50 °C in a closed 0.13 oz capacity glass jar. Prepared PNIPAM films on quartz substrates were exposed to 365 nm UV radiation using a UV illumination system (Newport, Model 97434). Conversion of AAmBP was monitored as a function of UV dose with a Hitachi U-3010 spectrophotometer in absorbance mode over a wavelength range of 200−800 nm. Due to differences in the spectral profiles, a given dose corresponds to different extents of benzophenone conversion using the two lamps. To correct for this difference, the swelling ratio was determined as a function of dose for both lamps (Supporting Information Figure S1) and used to convert doses from one lamp to the other. Doses stated in this work correspond to those measured for the X-Cite light source. The shear modulus of PAAm hydrogels was measured using a rheometer (Kinexus Pro+, Malvern) with 8 or 20 mm diameter stainless steel parallel plates; the storage modulus was determined at 1 Hz and 3% strain.

RESULTS AND DISCUSSION

We report here a method for mechanical characterization of thin polymer films inspired by previous work on capillary folding.[38,42,43] As first shown by Py et al.,[38] when a liquid droplet supported on a thin solid film is reduced in volume, and the contact line remains pinned at the film boundaries, interfacial tension is sufficient to wrap the sheet into a "closed" state, where opposite edges or corners of the film are brought into contact. The minimum in-plane size of the sheet required for wrapping is given by $L^* = SL_{EC} = S(B/\gamma)^{1/2}$ where S is a prefactor that depends on the geometric shape of the sheet.[38,44] Importantly, the value of S is anticipated to be *independent of the contact angle* of the liquid droplet on the sheet, due to the pinning of the contact line at the sheet edge. This means that once S is determined for a given shape, a simple measurement of L^* using any probe fluid that has a known (or measurable) value of surface tension γ with the medium can directly reveal the bending stiffness B of the film, which for a homogeneous and isotropic elastic material of thickness h and plane-strain modulus $\overline{E}$ is given by $\overline{E}h^3/12$.

Calibration of the Method. To establish the method, we used samples of a commercial polyimide film (Kapton 30 HN, $h = 7.6$ μm) of known plane-strain modulus ($\overline{E} = 2.83$ GPa) cut into square or equilateral triangles with a range of side lengths L. Due to the excellent chemical resistance of the polyimide film, it was possible to use a variety of liquid droplets, and continuous fluid phases (including air and liquids), giving rise to three-phase advancing contact angles ranging from 65 to 115° (Supporting Information Table S1). The film was placed at the interface of a droplet with a size substantially larger than L, allowing the entire surface of the film to be wet with very small initial curvature (Figure 2a,d). Unlike in previous

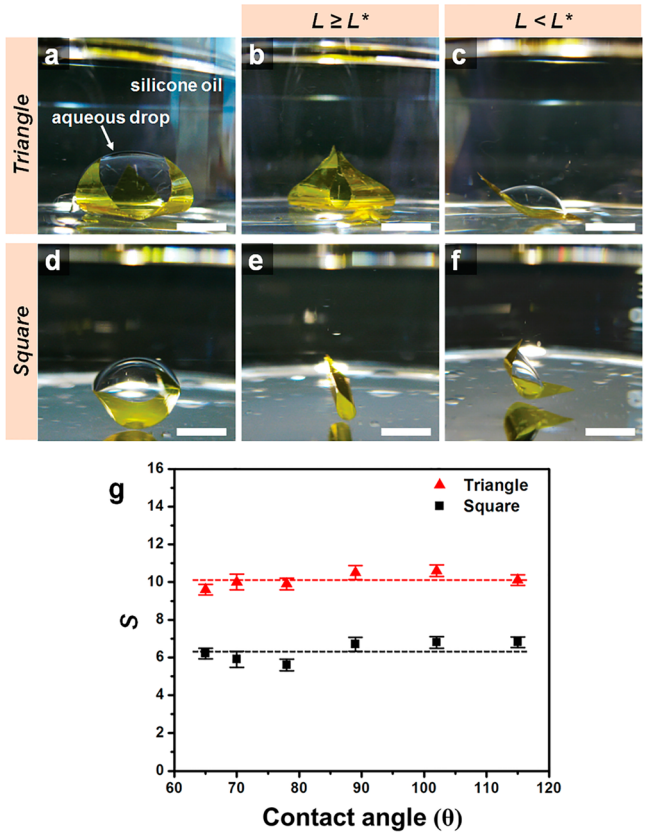

Figure 2. Calibration of geometric prefactors and contact angle effects. (a) A triangular polyimide sheet (Kapton 30 HN; $h = 7.6$ μm) was placed at the interface of an aqueous droplet and the silicone oil medium. Upon reducing the droplet volume by pipetting, (b) a film with $L = 21$ mm continually bent until opposing vertices contacted each other, indicating that $L > L^*$. In contrast, (c) a triangular film with $L = 13$ mm unbent before the vertices met, indicating that $L < L^*$. (d) Similarly, a square sheet with (e) $L = 11$ mm bent until opposite sides were contacting, while (f) one with $L = 9$ mm did not. All scale bars are 5 mm. (g) The measured prefactor S for triangles and squares is confirmed to be independent of advancing contact angle of the liquid/solid/medium interface.

experiments relying on evaporation,[38] here we reduce the volume of the droplet by pipetting, enabling the use of nonvolatile fluids, and increasing the speed of the experiments.

For films with sufficiently large L, a reduction in droplet volume caused the film to bend until opposite edges or corners met, for example as shown in Figure 2b,e, and Supporting Information Movie S1. These samples were taken to have $L > L^*$. By contrast, films with smaller L showed some degree of initial bending, but reopened to a flat state without contact of opposing edges/corners (Figure 2c,f and Supporting Information Movie S2). These samples were taken to have $L < L^*$. In many cases, the behavior followed that described by Py et al.;[38] i.e., the films were initially bent by surface tension, but with

DOI: 10.1021/acsami.5b02567
ACS Appl. Mater. Interfaces 2015, 7, 14734−14742

further reductions in drop volume they began to reopen before depinning of the drop. In some cases, however, especially for square geometries, depinning of the drop from the sheet edges was found to drive the reopening behavior, a point to which we will return later. By measuring polyimide sheets of several lengths, values of L^* were estimated and the corresponding prefactors S evaluated for both triangle and square geometries and for six different liquid drop/media pairs. As shown in Figure 2g, S was found to be independent of contact angle over the range studied, with average values of 10.1 ± 0.4 for triangles and 6.3 ± 0.5 for squares, compared to the respective literature values[38] of S = 11.9 and 7.0.

The possibility for the droplet to depin from the film edges introduces additional complexity to the problem, as studied in several previous reports.[45−47] Especially for real three-dimensional geometries, the influence of depinning on the transition from folded to unfolded states is not completely understood. According to calculations on two-dimensional,[45] and simplified three-dimensional, geometries,[46,47] however, the qualitative effect of depinning should be to cause an *overestimate* of L^* (and therefore S), due to the premature opening of the film in comparison to the pinned state. Further, this effect should become more pronounced with greater contact angle, since the drop can depin earlier in the process of liquid withdrawal. Since the values of S measured here are very close to, but slightly *lower than*, those reported previously in the absence of depinning, and furthermore are independent of contact angle, we conclude that depinning has a quite modest effect on estimates of L^*, at least for contact angles in the range studied.

A second possible source of systematic error in the method arises from the assumption that gravitational effects can be ignored. For the polyimide sheets studied here, L^* is similar to the gravitocapillary length $L_{GC} = (\gamma/\rho g)^{1/2}$, where ρ is the liquid buoyant density and g is gravitational acceleration (e.g., L_{GC} = 12 mm, while L^* = 10.5 ± 0.5 mm for squares and 16.5 ± 0.5 mm for triangles in the case of an aqueous droplet in the silicone oil medium), calling this assumption into question. However, we verified that the measured values of L^* did not depend on the placement of the sheet on the top, bottom, or side of the droplet, and thus we conclude that gravitational effects can safely be ignored, although this would not be the case for substantially larger values of L^* relative to L_{GC}.[38,45,47,48]

Finally, we note that, under certain conditions, two different stable configurations of the sheet and drop are possible,[46−48] and thus mechanical perturbation of the sample could force the system into a competing stable state that does not follow the expected behavior (i.e., a closed state for $L < L^*$ or an open state for $L > L^*$). To minimize the likelihood of pushing the system from one stable state to another, pipetting of the liquid was conducted gently. Once again, the consistency of the measured values of S across several different probe fluids argues strongly that this possible bistability does not unduly influence our results, but especially for samples with L very close to L^*, we cannot exclude the possibility that there is a small effect.

Characterization of Sub-millimeter-Scale Photopatterned Polymer Films. Having calibrated the method, we next turn to samples with previously uncharacterized mechanical properties. A topic of recent interest has been the patterning of small-scale three-dimensional structures by buckling of micropatterned two-dimensional polymer sheets due to in-plane or through-thickness variations in stress.[2−4,39,49−57] Although the contrast in modulus of the constituent materials plays an important role in determining the shapes formed in these ways, independent measurements of the elastic properties in such systems can often be challenging, and thus new methods for quantitatively measuring the properties of microscale polymer sheets would be valuable. To demonstrate the utility of elastocapillary bending measurements in this context, we next studied two different photo-cross-linkable polymers that have recently been used by our group[58,59] and others[60,61] to fabricate sub-millimeter-scale buckled and self-folding sheets.

We first consider a rigid glassy copolymer of *p*-methylstyrene (PpMS) containing pendent benzophenone (BP) photo-cross-linkers. Because our approach for patterning these materials involves releasing the sheet into an aqueous medium as the final step, we chose perfluorooctane (PFO) as a water-immiscible droplet phase that would not swell or plasticize the PpMS sheets. Based on a literature value of 3.8 GPa for the plane-strain modulus of polystyrene[62] (which presumably has elastic properties similar to PpMS), and a value of γ = 0.058 N/m for the PFO/aqueous solution interface (measured by pendent drop tensiometry), we estimated that a film thickness of $h \approx 1$ μm should yield values of $L^* \sim 1$ mm, matching the sizes that can be conveniently photopatterned. However, to test this prediction, we first prepared sheets with several different thicknesses, as summarized in Figure 3. For a thickness of h =

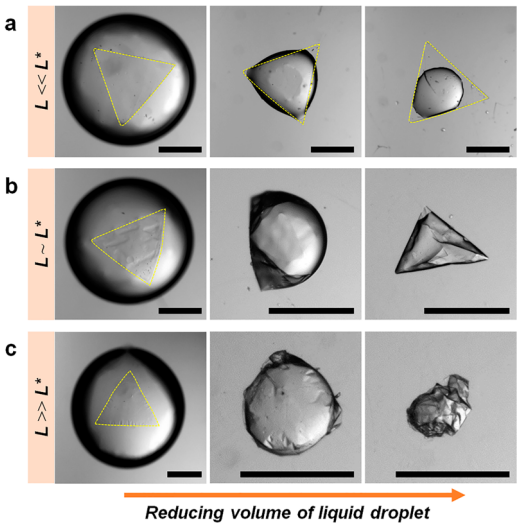

Figure 3. Elastocapillary bending measurements of glassy PpMS sheets. Optical micrographs of PpMS sheets with side lengths L = 1 mm and different thicknesses h at the PFO/aqueous medium interface. Upon reducing the volume of the PFO droplet, PpMS sheets with (a) h = 2 μm remain nearly flat, while (b) those with h = 0.67 μm wrap the droplet and (c) those with h = 0.12 μm crumple. All scale bars are 500 μm.

2.0 μm, interfacial tension was insufficient to bend 1-mm-sized sheets, corresponding to $L \ll L^*$, while for a thickness of h = 0.12 μm, sheets became highly crumpled[63] upon removing PFO, corresponding to $L \gg L^*$. An intermediate thickness of h = 0.67 μm, however, yielded wrapping of droplets in a manner consistent with $L \sim L^*$.

Having identified an appropriate film thickness for elastocapillary bending measurements, we fixed h = 0.67 μm and prepared a series of square and equilateral triangle shapes with side lengths varying from 0.2 to 1.0 mm in 0.1 mm increments. Using a microcapillary to remove PFO from droplets with interfacially adsorbed PpMS sheets, and an optical

DOI: 10.1021/acsami.5b02567
ACS Appl. Mater. Interfaces 2015, 7, 14734−14742

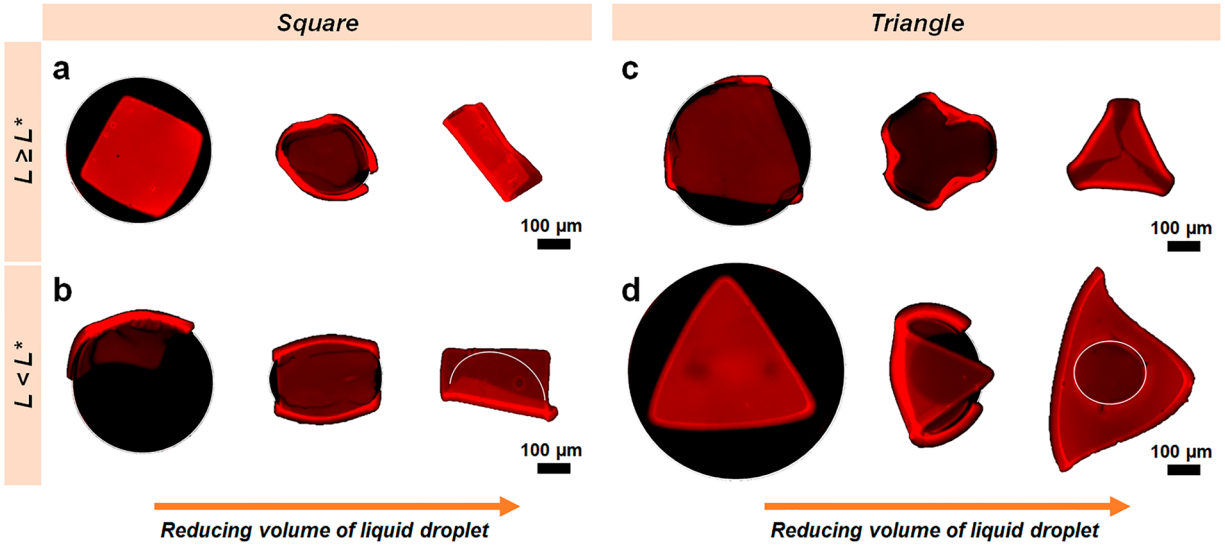

Figure 4. Elastocapillary bending of measurements of PNIPAM hydrogel sheets. Fluorescence micrographs of cross-linked hydrogels at the interface of a PFO droplet (black in color or denoted by a white line) and the aqueous medium. Square and triangle sheets (a, c) wrapping the droplet for $L \geq L^*$ and (b, d) unbending for $L < L^*$, during microcapillary suction of PFO droplets.

microscope to visualize the deformation, we determined values of $L^* = 450 \pm 50$ μm for triangles and 250 ± 50 μm for squares from the minimum/maximum values of L for which wrapping/reopening was observed. For triangles, reopening primarily occurred prior to depinning of the drop, while for squares, depinning of the drop from the sheet edges was observed.

The corresponding values of plane-strain modulus estimated from eq 1 were 4.6 ± 1.0 and 3.8 ± 1.4 GPa, in good agreement with expectations based on the literature value for polystyrene. The uncertainties in these values are dominated by the variations in size L used, and thus can be reduced by using samples more closely spaced in size, as we demonstrate for several samples below. However, reducing the uncertainty below ±5% would require more precise measurements of the prefactor S, and ultimately we expect that the precision of the method can be limited in the ability to unambiguously resolve "open" from "closed" states, as well as possible influences of depinning, gravity, and multistability. To compare these values with those from an established technique on the same materials, nanoindentation experiments were also performed on PpMS sheets prepared with a much greater thickness ($h \sim 100$ μm) to minimize the influence of the underlying rigid substrate. Values of $\bar{E} = 5.0 \pm 0.1$ and 5.9 ± 0.1 GPa were measured for two separately prepared samples, in reasonably good agreement with the results from elastocapillary bending tests (Supporting Information Table S2). Given its simplicity from the perspective of instrumentation and analysis, capillary bending can thus provide an attractive alternative to nanoindentation for the characterization of glassy polymer films in the appropriate thickness range.

Next, to demonstrate the applicability of the method for softer materials, we characterized films of a photo-cross-linkable poly(*N*-isopropylacrylamide-*co*-acrylic acid) (PNIPAM) copolymer cross-linked to different extents. Given the submillimeter-scale dimensions of these samples, it has not previously been possible to characterize their elastic moduli by conventional methods such as tensile testing or shear rheology. While characterization by AFM-based nanoindentation should be possible, our efforts in this regard have been complicated by tip/sample adhesion issues and relatively slow time scales for stress relaxation. Thus, capillary bending represents a promising method for characterization of these materials.

Based on the content of photo-cross-linker in the copolymer, expected moduli are in the range of 100 kPa to 1 MPa, and thus we estimated from eq 1 that sheets with $h \approx 20-30$ μm and $L \sim 1$ mm would be appropriate. Films with dry thicknesses of $h_0 = 8-13$ μm were prepared by solution-casting and photopatterned into square or equilateral triangular shapes with dry side lengths of $L_0 = 0.2-0.6$ mm using a UV dose sufficient to convert only a fraction of the benzophenone units. The sheets were then allowed to swell to equilibrium in a low ionic strength aqueous buffer (1 mM NaCl and 1 mM phosphate buffer, pH 7.2) at room temperature, and the volumetric swelling $Q = (L/L_0)^3$ was determined using an optical microscope to measure the change in size (where we separately verified that the swelling is isotropic by also measuring the change in thickness for selected samples). Doses ranging from 3 to 30 mJ/cm^2 were employed, resulting in values of Q from 15.8 to 3.5. As summarized in Figure 4, PNIPAM sheets were placed at the interface between a PFO droplet and the aqueous medium, and the droplet volume was reduced using microcapillary suction (see Supporting Information Movies S3 and S4). The values of $\bar{E}$ were determined by the transition from wrapped to reopened states via eq 1 as before, although in this case both L and h of the sheets were varied (due to the sample-to-sample variation in thickness obtained by drop-casting). Furthermore, we combined data for both squares and triangles to obtain a single estimate of $\bar{E}$ with lower uncertainty. The values of $\bar{E}$ for the swelled hydrogel sheets ranged from 200 to 800 kPa with increasing cross-link density, as summarized in Supporting Information Table S3. As with PpMS sheets, triangular PNIPAM sheets primarily showed reopening before depinning, whereas depinning was typically observed for square sheets.

To better understand how the modulus and swelling ratio of the gel sheets depend on cross-linking, we used UV−vis spectroscopy to characterize how the conversion p of benzophenone units increased as a function of UV dose. Specifically we monitored the decay of the $\pi-\pi^*$ absorption

DOI: 10.1021/acsami.5b02567
ACS Appl. Mater. Interfaces 2015, 7, 14734−14742

peak at 300 nm after normalization at the isosbestic point (Supporting Information Figure S2), using a previously described procedure.[58] Assuming that each benzophenone unit has an equal probability of forming a cross-link, p should be inversely proportional to the length N of polymer strands in the cross-linked network. In Figure 5, we plot both $\bar{E}$ and Q as

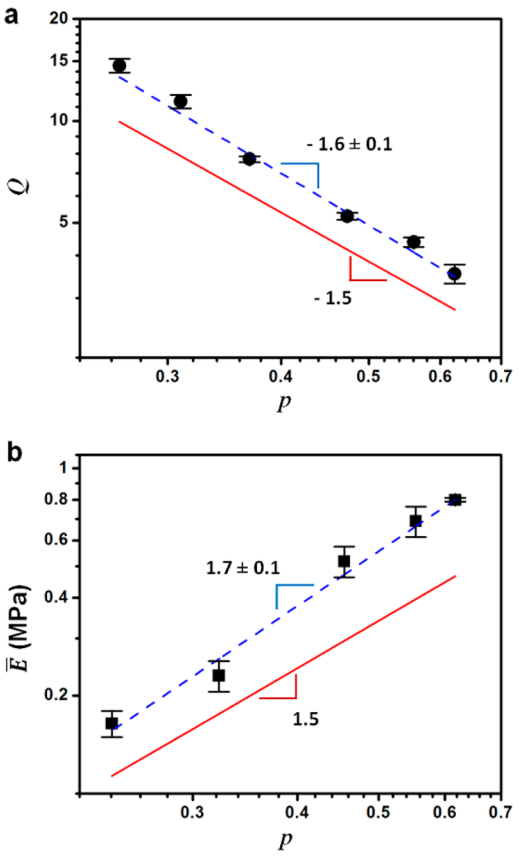

Figure 5. Swelling ratios and moduli of hydrogels as a function of cross-linking. Logarithmic scales are used for both axes for the plots in a and b, and predicted scaling exponents are drawn as solid lines. (a) Plotting the volumetric swelling ratio (Q) against the conversion of photo-cross-linker (p) reveals a best-fit slope (dashed line) of -1.6 ± 0.1 close to the predicted power law of -1.5. (b) Plotting the plane-strain modulus ($\bar{E}$) against the relative conversion of photo-cross-linker (p) reveals a best-fit slope of 1.7 ± 0.1 (dashed line) close to the predicted power law of 1.5 for the shear modulus.

functions of p. The relationship between Q and p can be well-described by a power law dependence $Q \sim p^a$ with a best-fit exponent of $a = -1.6 \pm 0.1$, which is in good agreement with the theoretically predicted exponent of -1.5 for polyelectrolyte gels at low salt concentration.[64] The modulus values measured by elastocapillary bending are also consistent with power law behavior $\bar{E} \sim p^b$ with a best-fit exponent of $b = 1.7 \pm 0.1$ that is slightly larger than the predicted exponent for the shear modulus of 1.5, although this agreement is reasonable in light of the modest range of p studied, and the likelihood that Poisson's ratio ν, where $\bar{E} = 2G/(1 - \nu)$, also increases slightly with increasing cross-link density. While the dependence of $\bar{E}$ and Q separately on cross-link density has not previously been widely studied for polyelectrolyte gels, the prediction $G \sim Q^{-1}$ has been verified in several previous reports,[64−66] and within uncertainty, the data reported here also support the dependence $\bar{E} \sim Q^{-1}$.

Characterization of Soft Hydrogels. Finally, to prove the suitability of elastocapillary bending to characterize even very soft polymer films ($\bar{E} \sim 10^3$ Pa), polyacrylamide (PAAm) hydrogel layers with centimeter-scale lateral dimensions were prepared by photoinitiated polymerization in aqueous solution. The technique allows for a simple measurement of the elastic modulus in the fully swelled state, which can be challenging using conventional shear rheology due to the possibility for slip between the hydrated gel surface and the rheometer plate. Swelled PAAm gel sheets (volumetric swelling ratio, 1.3) were placed at the interface of a water droplet and silicone oil medium, and the water droplet volume reduced by pipetting (Figure 6) to determine a value of $L^* = 21.5 \pm 0.5$ mm for

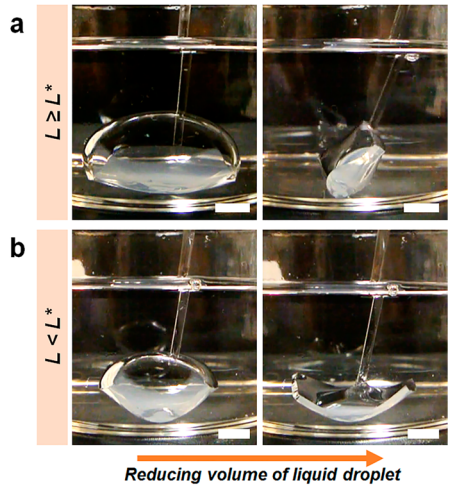

Figure 6. Elastocapillary bending of measurements of swelled polyacrylamide (PAAm) hydrogel sheets. Photographs of PAAm hydrogels at the interface of a water droplet and the silicone oil medium. A square sheet (a) wrapping the droplet for $L \geq L^*$ and (b) unbending for $L < L^*$, as the droplet volume is reduced by pipetting. All scale bars are 5 mm.

squares with $h = 1$ mm. In this case, we used only square sheets, which showed clear reopening before depinning of the drop. In light of the large in-plane dimensions of these sheets, we also verified that the measured value of L^* was independent of the orientation of the drop, indicating that gravity can safely be ignored. Consequently, from eq 1, we estimate $\bar{E} = 5.6 \pm 0.3$ kPa. From shear rheology on PAAm gels in the unswelled state (Supporting Information Table S4), we determined a shear modulus of $G = 2.5 \pm 0.4$ kPa. Unfortunately, only a rough comparison of these two values via the relationship $\bar{E} = 2G/(1 - \nu)$ is possible, since we have measured neither the Poisson ratio ν nor how much the gel's elastic modulus decreases due to swelling. However, since the elastocapillary measurement is conducted over a time scale of ~60 s, substantially shorter than the poroelastic relaxation time (estimated to be $\sim 10^4$ s for a thickness of 1 mm[67]), we expect that the effective value of ν is close to 0.5. With this assumption, the values from shear rheology would correspond to $\bar{E} = 10.0 \pm 1.6$ kPa. Based on a volumetric swelling of 1.3 compared to the as-prepared state, and the scaling prediction[68] for flexible polymer networks in good solvents $G \sim \phi^{7/12}$, with ϕ as the polymer volume fraction, we can estimate that swelling should reduce this value to $\bar{E} = 8.6 \pm 1.4$ kPa. This value is not in quantitative agreement with that from elastocapillary bending but is reasonably close, especially in light of the assumptions

DOI: 10.1021/acsami.5b02567
ACS Appl. Mater. Interfaces 2015, 7, 14734−14742

necessary to make this comparison. We note that the ability to directly characterize the modulus of gels in the equilibrium swelled state, which is typically difficult using shear rheology due to slip between the gel surface and the rheometer plate, is an attractive feature of the elastocapillary bending method.

Range of Applicability of the Method. In Figure 7, we summarize the broad range of applicability of this technique via

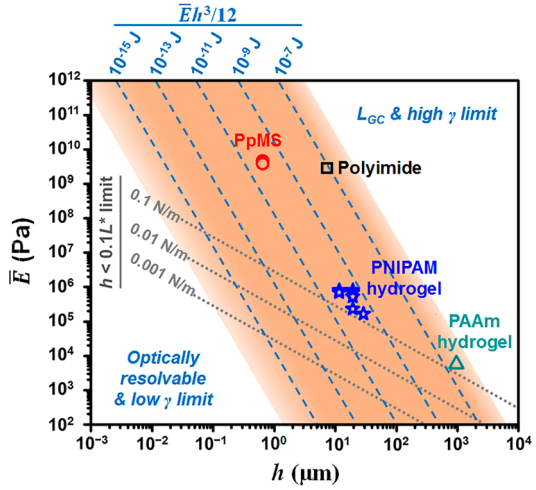

Figure 7. Accessible regions for elastocapillary bending measurements. Logarithmic scales are used for the plane-strain modulus ($\bar{E}$) and thickness (h) axes. The lines of slope −3 (blue dashed lines) correspond to constant values of bending modulus ($\bar{E}h^3/12$), and the shaded region represents the region accessible for square geometries using realistic values of critical sheet dimensions L^* and surface tension γ. The gray dotted lines of slope −1 correspond to constant values of $\bar{E}h$ corresponding to the thin film limit $h < 0.1L^*$ for the indicated values of γ. The samples characterized here are plotted as symbols.

a log−log plot denoting the range of accessible values (shaded in orange) of $\bar{E}$ and h for sheets of square geometry. The blue dashed lines of slope −3 correspond to constant values of bending modulus $\bar{E}h^3/12$ (or equivalently, $\gamma L^{*2}/S^2$). The upper-right end of the shaded regime corresponds to a maximum sheet size of $L^* \approx 10$ mm dictated by the gravitocapillary length, along with a surface tension of up to $\gamma \approx 0.1$ N/m achievable using typical liquids in contact with air. Similarly, the lower-left end is determined from the in-plane dimensions easily observable by optical techniques $L^* \approx 10$ μm, and a minimum surface tension of $\gamma \approx 1$ mN/m that can be achieved for weakly immiscible fluids or by adding surfactants. These values of L^* and γ represent a range of 8 orders of magnitude in bending modulus (from $\sim 10^{-15}$ to 10^{-7} J) that can be reasonably accessed by the technique. Presumably, the use of alternative sheet geometries, density matched liquids, very high or low interfacial tension fluids, and/or high resolution imaging methods could extend this range further in both directions, as denoted by the gradient regions surrounding the shaded region in Figure 7. However, even based on currently feasible experiments, the technique can be applied to characterize films of the stiffest known materials ($\bar{E} \sim 1$ TPa) with thicknesses in the range of ∼3 nm to 3 μm, as well as the softest solids ($\bar{E} \sim 100$ Pa) with thicknesses near 1 mm.

Another important constraint on the method is that the film must be thin, i.e., $h \ll L^*$, so that the strains induced by bending are small and linear elasticity can reasonably be applied. Using $h = 0.1L^*$ as a maximum tolerable thickness, eq 1 becomes $\bar{E}h > 1200\ \gamma/S^2$, a constraint denoted by the dotted gray lines of slope −1 in Figure 7. For each line (corresponding to values of $\gamma = 0.001$, 0.01, and 0.1 N/m), the region above and to the right is accessible, while that below and to the left is not. This consideration dictates that for soft materials ($\bar{E} \sim 100$ Pa to 1 MPa), the combination of a relatively low surface tension fluid and a large thickness is necessary to ensure that the strains induced by surface tension remain modest.

CONCLUSIONS

We have developed an elastocapillary bending approach to measure elastic moduli in the range of kilopascals to gigapascals for polymer films, including those with sub-millimeter-scale dimensions and immersed in liquid media. The method requires only separate measurements of the liquid/air or liquid/liquid interfacial tension and the sheet thickness and involves simple and rapid measurements not requiring any special equipment.

One important limitation of the method is that it requires testing of a series of samples with different in-plane dimensions, which may not always be practical. Further developments that allow for *in situ* variation of surface tension using a surfactant or applied electric potential could potentially enable similar measurements with only a single sample. Alternatively, since the elastic films are not damaged during testing, the use of a series of probe fluids of varying surface tension could allow for characterization using a single sample. The use of a "racket" geometry, where a thin strip of the film is held together at its free ends by the meniscus of a wetting liquid, could also allow for a direct measurement of L_{EC} using a single sample,[38] although preparing a film in this geometry would require direct physical manipulation of the film to place the ends in contact. For samples that are sufficiently large and robust to withstand such handling, this may represent a more attractive alternative than the method described here, while for very small, flexible, or fragile films, we expect that the current method is better suited. In addition, a full exploration of the bifurcation diagrams accounting for gravitational effects and depinning[45] would be valuable to guide future use of the method.

However, in light of the simplicity of the measurements, the broad range of moduli that can be accessed, and the applicability for samples with small dimensions in liquid environments, we expect that elastocapillary bending will prove to be a valuable and versatile method for measuring the elastic modulus of flexible thin films. While we have investigated only homogeneous elastic films here, the method should be more broadly applicable for determining the bending stiffness of composites, laminates, and (with suitable choices of film geometry) materials with in-plane anisotropy.

ASSOCIATED CONTENT

Supporting Information

Data of droplet and continuous phases for calibration of geometric prefactors, data of elastocapillary bending tests with PNIPAM hydrogel sheets, data of nanoindentation of PpMS films and shear rheology test of PAAm films, the swelling ratio of PNIPAM with different light sources, conversion of BP as a function of UV dose, and captions of supporting movies showing elastocapillary bending of Kapton and hydrogel films. The Supporting Information is available free of charge on the ACS Publications website at DOI: 10.1021/acsami.5b02567.

DOI: 10.1021/acsami.5b02567
ACS Appl. Mater. Interfaces 2015, 7, 14734−14742

AUTHOR INFORMATION

Corresponding Author

*E-mail: hayward@umass.edu.

Notes

The authors declare no competing financial interest.

ACKNOWLEDGMENTS

We thank Arthur A. Evans for helpful discussions. This research was funded by the Army Research Office through Grant W911NF-11-1-0080.

REFERENCES

(1) Sharon, E.; Efrati, E. The Mechanics of Non-Euclidean Plates. *Soft Matter* **2010**, *6*, 5693−5704.
(2) Chen, D.; Yoon, J.; Chandra, D.; Crosby, A. J.; Hayward, R. C. Stimuli-Responsive Buckling Mechanics of Polymer Films. *J. Polym. Sci., Part B: Polym. Phys.* **2014**, *52*, 1441−1461.
(3) Ionov, L. Biomimetic Hydrogel-Based Actuating Systems. *Adv. Funct. Mater.* **2013**, *23*, 4555−4570.
(4) Gracias, D. H. Stimuli Responsive Self-Folding Using Thin Polymer Films. *Curr. Opin. Chem. Eng.* **2013**, *2*, 112−119.
(5) Mitragotri, S.; Lahann, J. Physical Approaches to Biomaterial Design. *Nat. Mater.* **2009**, *8*, 15−23.
(6) Stuart, M. A. C.; Huck, W. T. S.; Genzer, J.; Muller, M.; Ober, C.; Stamm, M.; Sukhorukov, G. B.; Szleifer, I.; Tsukruk, V. V.; Urban, M.; Winnik, F.; Zauscher, S.; Luzinov, I.; Minko, S. Emerging Applications of Stimuli-Responsive Polymer Materials. *Nat. Mater.* **2010**, *9*, 101−113.
(7) Chen, X.; Yin, J. Buckling Patterns of Thin Films on Curved Compliant Substrates with Applications to Morphogenesis and Three-Dimensional Micro-Fabrication. *Soft Matter* **2010**, *6*, 5667−5680.
(8) Studart, A. R.; Erb, R. M. Bioinspired Materials That Self-Shape through Programmed Microstructures. *Soft Matter* **2014**, *10*, 1284−1294.
(9) VanLandingham, M. R.; Villarrubia, J. S.; Guthrie, W. F.; Meyers, G. F. Nanoindentation of Polymers: An Overview. *Macromol. Symp.* **2001**, *167*, 15−43.
(10) Geng, K. B.; Yang, F. Q.; Druffel, T.; Grulke, E. A. Nanoindentation Behavior of Ultrathin Polymeric Films. *Polymer* **2005**, *46*, 11768−11772.
(11) Du, B.; Tsui, O. K. C.; Zhang, Q.; He, T. Study of Elastic Modulus and Yield Strength of Polymer Thin Films Using Atomic Force Microscopy. *Langmuir* **2001**, *17*, 3286−3291.
(12) Hu, Y. H.; You, J. O.; Auguste, D. T.; Suo, Z. G.; Vlassak, J. J. Indentation: A Simple, Nondestructive Method for Characterizing the Mechanical and Transport Properties of pH-Sensitive Hydrogels. *J. Mater. Res.* **2012**, *27*, 152−160.
(13) Drira, Z.; Yadavalli, V. K. Nanomechanical Measurements of Polyethylene Glycol Hydrogels Using Atomic Force Microscopy. *J. Mech. Behav. Biomed.* **2013**, *18*, 20−28.
(14) Gupta, S.; Greeshma, T.; Basu, B.; Goswami, S.; Sinha, A. Stiffness- and Wettability-Dependent Myoblast Cell Compatibility of Transparent Poly(Vinyl Alcohol) Hydrogels. *J. Biomed. Mater. Res., Part B* **2013**, *101B*, 346−354.
(15) Alonso, J. L.; Goldmann, W. H. Feeling the Forces: Atomic Force Microscopy in Cell Biology. *Life Sci.* **2003**, *72*, 2553−2560.
(16) Ren, J.; Zou, Q. Z. A Control-Based Approach to Accurate Nanoindentation Quantification in Broadband Nanomechanical Measurement Using Scanning Probe Microscope. *IEEE Trans. Nanotechnol.* **2014**, *13*, 46−54.
(17) Rettler, E.; Hoeppener, S.; Sigusch, B. W.; Schubert, U. S. Mapping the Mechanical Properties of Biomaterials on Different Length Scales: Depth-Sensing Indentation and AFM Based Nanoindentation. *J. Mater. Chem. B* **2013**, *1*, 2789−2806.
(18) Demichelis, A.; Pavarelli, S.; Mortati, L.; Sassi, G.; Sassi, M. Study on the AFM Force Spectroscopy Method for Elastic Modulus Measurement of Living Cells. *J. Phys.: Conf. Ser.* **2013**, *459*, 012050.
(19) Vinckier, A.; Semenza, G. Measuring Elasticity of Biological Materials by Atomic Force Microscopy. *FEBS Lett.* **1998**, *430*, 12−16.
(20) Ebenstein, D. M.; Pruitt, L. A. Nanoindentation of Biological Materials. *Nano Today* **2006**, *1*, 26−33.
(21) Kaufman, J. D.; Klapperich, C. M. Surface Detection Errors Cause Overestimation of the Modulus in Nanoindentation on Soft Materials. *J. Mech. Behav. Biomed.* **2009**, *2*, 312−317.
(22) Gianola, D. S.; Eberl, C. Micro- and Nanoscale Tensile Testing of Materials. *JOM* **2009**, *61*, 24−35.
(23) Hemker, K. J.; Sharpe, W. N. Microscale Characterization of Mechanical Properties. *Annu. Rev. Mater. Res.* **2007**, *37*, 93−126.
(24) Chasiotis, I.; Knauss, W. G. A New Microtensile Tester for the Study of MEMS Materials with the Aid of Atomic Force Microscopy. *Exp. Mech.* **2002**, *42*, 51−57.
(25) Vlassak, J. J.; Nix, W. D. A New Bulge Test Technique for the Determination of Young Modulus and Poisson Ratio of Thin-Films. *J. Mater. Res.* **1992**, *7*, 3242−3249.
(26) Xiang, Y.; Chen, X.; Vlassak, J. J. Plane-Strain Bulge Test for Thin Films. *J. Mater. Res.* **2005**, *20*, 2360−2370.
(27) Evans, E. A.; Waugh, R.; Melnik, L. Elastic Area Compressibility Modulus of Red-Cell Membrane. *Biophys. J.* **1976**, *16*, 585−595.
(28) Mabrouk, E.; Cuvelier, D.; Pontani, L.-L.; Xu, B.; Levy, D.; Keller, P.; Brochard-Wyart, F.; Nassoy, P.; Li, M.-H. Formation and Material Properties of Giant Liquid Crystal Polymersomes. *Soft Matter* **2009**, *5*, 1870−1878.
(29) Wyss, H. M.; Franke, T.; Mele, E.; Weitz, D. A. Capillary Micromechanics: Measuring the Elasticity of Microscopic Soft Objects. *Soft Matter* **2010**, *6*, 4550−4555.
(30) Wyss, H. M.; Henderson, J. M.; Byfield, F. J.; Bruggeman, L. A.; Ding, Y. X.; Huang, C. F.; Suh, J. H.; Franke, T.; Mele, E.; Pollak, M. R.; Miner, J. H.; Janmey, P. A.; Weitz, D. A.; Miller, R. T. Biophysical Properties of Normal and Diseased Renal Glomeruli. *Am. J. Physiol.-Cell Ph.* **2011**, *300*, C397−C405.
(31) Luo, Y. N.; Chen, D. Y.; Zhao, Y.; Wei, C.; Zhao, X. T.; Yue, W. T.; Long, R.; Wang, J. B.; Chen, J. A Constriction Channel Based Microfluidic System Enabling Continuous Characterization of Cellular Instantaneous Young's Modulus. *Sens. Actuators, B* **2014**, *202*, 1183−1189.
(32) Zimberlin, J. A.; Sanabria-DeLong, N.; Tew, G. N.; Crosby, A. J. Cavitation Rheology for Soft Materials. *Soft Matter* **2007**, *3*, 763−767.
(33) Chin, M. S.; Freniere, B. B.; Fakhouri, S.; Harris, J. E.; Lalikos, J. F.; Crosby, A. J. Cavitation Rheology as a Potential Method for in Vivo Assessment of Skin Biomechanics. *Plast. Reconstr. Surg.* **2013**, *131*, 303e−305e.
(34) Cui, J.; Lee, C. H.; Delbos, A.; McManus, J. J.; Crosby, A. J. Cavitation Rheology of the Eye Lens. *Soft Matter* **2011**, *7*, 7827−7831.
(35) Stafford, C. M.; Harrison, C.; Beers, K. L.; Karim, A.; Amis, E. J.; VanLandingham, M. R.; Kim, H.-C.; Volksen, W.; Miller, R. D.; Simonyi, E. E. A Buckling-Based Metrology for Measuring the Elastic Moduli of Polymeric Thin Films. *Nat. Mater.* **2004**, *3*, 545−550.
(36) Huang, J.; Juszkiewicz, M.; de Jeu, W. H.; Cerda, E.; Emrick, T.; Menon, N.; Russell, T. P. Capillary Wrinkling of Floating Thin Polymer Films. *Science* **2007**, *317*, 650−653.
(37) Kim, J.-H.; Nizami, A.; Hwangbo, Y.; Jang, B.; Lee, H.-J.; Woo, C.-S.; Hyun, S.; Kim, T.-S. Tensile Testing of Ultra-Thin Films on Water Surface. *Nat. Commun.* **2013**, *4*, 2520.
(38) Py, C.; Reverdy, P.; Doppler, L.; Bico, J.; Roman, B.; Baroud, C. N. Capillary Origami: Spontaneous Wrapping of a Droplet with an Elastic Sheet. *Phys. Rev. Lett.* **2007**, *98*, 156103.
(39) Kim, J.; Hanna, J. A.; Byun, M.; Santangelo, C. D.; Hayward, R. C. Designing Responsive Buckled Surfaces by Halftone Gel Lithography. *Science* **2012**, *335*, 1201−1205.
(40) Linder, V.; Gates, B. D.; Ryan, D.; Parviz, B. A.; Whitesides, G. M. Water-Soluble Sacrificial Layers for Surface Micromachining. *Small* **2005**, *1*, 730−736.
(41) Oliver, W. C.; Pharr, G. M. An Improved Technique for Determining Hardness and Elastic-Modulus Using Load and Displacement Sensing Indentation Experiments. *J. Mater. Res.* **1992**, *7*, 1564−1583.

DOI: 10.1021/acsami.5b02567
ACS Appl. Mater. Interfaces 2015, 7, 14734−14742

(42) Roman, B.; Bico, J. Elasto-Capillarity: Deforming an Elastic Structure with a Liquid Droplet. *J. Phys.: Condens. Matter* **2010**, *22*, 493101.
(43) Guo, X. Y.; Li, H.; Ahn, B. Y.; Duoss, E. B.; Hsia, K. J.; Lewis, J. A.; Nuzzo, R. G. Two- and Three-Dimensional Folding of Thin Film Single-Crystalline Silicon for Photovoltaic Power Applications. *Proc. Natl. Acad. Sci. U. S. A.* **2009**, *106*, 20149−20154.
(44) Li, H. A.; Guo, X. Y.; Nuzzo, R. G.; Hsia, K. J. Capillary Induced Self-Assembly of Thin Foils into 3Dstructures. *J. Mech. Phys. Solids* **2010**, *58*, 2033−2042.
(45) Neukirch, S.; Antkowiak, A.; Marigo, J. J. The Bending of an Elastic Beam by a Liquid Drop: A Variational Approach. *Proc. R. Soc. London, Ser. A* **2013**, *469*, 20130066.
(46) Antkowiak, A.; Audoly, B.; Josserand, C.; Neukirch, S.; Rivetti, M. Instant Fabrication and Selection of Folded Structures Using Drop Impact. *Proc. Natl. Acad. Sci. U. S. A.* **2011**, *108*, 10400−10404.
(47) de Langre, E.; Baroud, C. N.; Reverdy, P. Energy Criteria for Elasto-Capillary Wrapping. *J. Fluid. Struct.* **2010**, *26*, 205−217.
(48) Rivetti, M.; Neukirch, S. Instabilities in a Drop-Strip System: A Simplified Model. *Proc. R. Soc. London, Ser. A* **2012**, *468*, 1304−1324.
(49) Kim, J.; Hanna, J. A.; Hayward, R. C.; Santangelo, C. D. Thermally Responsive Rolling of Thin Gel Strips with Discrete Variations in Swelling. *Soft Matter* **2012**, *8*, 2375−2381.
(50) Byun, M.; Santangelo, C. D.; Hayward, R. C. Swelling-Driven Rolling and Anisotropic Expansion of Striped Gel Sheets. *Soft Matter* **2013**, *9*, 8264−8273.
(51) Wu, Z. L.; Moshe, M.; Greener, J.; Therien-Aubin, H.; Nie, Z.; Sharon, E.; Kumacheva, E. Three-Dimensional Shape Transformations of Hydrogel Sheets Induced by Small-Scale Modulation of Internal Stresses. *Nat. Commun.* **2013**, *4*, 1586.
(52) Therien-Aubin, H.; Wu, Z. L.; Nie, Z. H.; Kumacheva, E. Multiple Shape Transformations of Composite Hydrogel Sheets. *J. Am. Chem. Soc.* **2013**, *135*, 4834−4839.
(53) Ionov, L. 3D Microfabrication Using Stimuli-Responsive Self-Folding Polymer Films. *Polym. Rev.* **2013**, *53*, 92−107.
(54) Stoychev, G.; Zakharchenko, S.; Turcaud, S.; Dunlop, J. W. C.; Ionov, L. Shape-Programmed Folding of Stimuli-Responsive Polymer Bilayers. *ACS Nano* **2012**, *6*, 3925−3934.
(55) Alben, S.; Balakrisnan, B.; Smela, E. Edge Effects Determine the Direction of Bilayer Bending. *Nano Lett.* **2011**, *11*, 2280−2285.
(56) Malachowski, K.; Breger, J.; Kwag, H. R.; Wang, M. O.; Fisher, J. P.; Selaru, F. M.; Gracias, D. H. Stimuli-Responsive Theragrippers for Chemomechanical Controlled Release. *Angew. Chem., Int. Ed.* **2014**, *53*, 8045−8049.
(57) Fernandes, R.; Gracias, D. H. Self-Folding Polymeric Containers for Encapsulation and Delivery of Drugs. *Adv. Drug Delivery Rev.* **2012**, *64*, 1579−1589.
(58) Christensen, S. K.; Chiappelli, M. C.; Hayward, R. C. Gelation of Copolymers with Pendent Benzophenone Photo-Cross-Linkers. *Macromolecules* **2012**, *45*, 5237−5246.
(59) Chiappelli, M. C.; Hayward, R. C. Photonic Multilayer Sensors from Photo-Crosslinkable Polymer Films. *Adv. Mater.* **2012**, *24*, 6100−6104.
(60) Zakharchenko, S.; Puretskiy, N.; Stoychev, G.; Stamm, M.; Ionov, L. Temperature Controlled Encapsulation and Release Using Partially Biodegradable Thermo-Magneto-Sensitive Self-Rolling Tubes. *Soft Matter* **2010**, *6*, 2633−2636.
(61) Stoychev, G.; Puretskiy, N.; Ionov, L. Self-Folding All-Polymer Thermoresponsive Microcapsules. *Soft Matter* **2011**, *7*, 3277−3279.
(62) Brandrup, J.; Immergut, E. H. *Polymer Handbook*; Wiley: New York, 1989.
(63) King, H.; Schroll, R. D.; Davidovitch, B.; Menon, N. Elastic Sheet on a Liquid Drop Reveals Wrinkling and Crumpling as Distinct Symmetry-Breaking Instabilities. *Proc. Natl. Acad. Sci. U. S. A.* **2012**, *109*, 9716−9720.
(64) Rubinstein, M.; Colby, R. H.; Dobrynin, A. V.; Joanny, J.-F. Elastic Modulus and Equilibrium Swelling of Polyelectrolyte Gels. *Macromolecules* **1996**, *29*, 398−406.
(65) Dubrovskii, S. A.; Rakova, G. V. Elastic and Osmotic Behavior and Network Imperfections of Nonionic and Weakly Ionized Acrylamide-Based Hydrogels. *Macromolecules* **1997**, *30*, 7478−7486.
(66) Skouri, R.; Schosseler, F.; Munch, J. P.; Candau, S. J. Swelling and Elastic Properties of Polyelectrolyte Gels. *Macromolecules* **1995**, *28*, 197−210.
(67) Yoon, J.; Cai, S.; Suo, Z.; Hayward, R. C. Poroelastic Swelling Kinetics of Thin Hydrogel Layers: Comparison of Theory and Experiment. *Soft Matter* **2010**, *6*, 6004−6012.
(68) Obukhov, S. P.; Rubinstein, M.; Colby, R. H. Network Modulus and Superelasticity. *Macromolecules* **1994**, *27*, 3191−3198.

DOI: 10.1021/acsami.5b02567
ACS Appl. Mater. Interfaces 2015, 7, 14734−14742